Data-driven Modeling and Predictive Control of Combustion Phasing for RCCI Engines

B. K. Irdmousa[†], Syed Z. Rizvi^{††}, J. Mohammadpour Velni^{†††}, J. D. Naber[†], and M. Shahbakhti[†]

Abstract—Reactivity controlled compression ignition (RCCI) engines center on a combustion strategy with higher thermal efficiency, lower particulate matter (PM), and lower oxides of nitrogen (NOx) emissions compared to conventional diesel combustion (CDC) engines. However, real time optimal control of RCCI engines is challenging during transient operation due to the need for high fidelity combustion models. Development of a simple, yet accurate control-oriented RCCI model from physical laws is time consuming and often requires substantial calibrations. To overcome these challenges, data-driven models can be developed. In this paper, a data-driven linear parametervarying (LPV) model for an RCCI engine is developed. An LPV state space model is identified to predict RCCI combustion phasing as a function of multiple RCCI control variables. The results show that the proposed method provides a fast and reliable route to identify an RCCI engine model. The developed model is then used for the design of a model predictive controller (MPC) to control crank angle for 50% fuel burnt (CA50) for varying engine conditions. The experimental results show that the designed MPC with the data-driven LPV model can track desired CA50 with less than 1 crank angle degree (CAD) error against changes in engine load.

I. INTRODUCTION

RCCI is a dual fuel low temperature combustion (LTC) strategy for internal combustion engines (ICE) which runs with a blend of a low reactive fuel and a high reactive fuel. It offers higher fuel conversion efficiency at lower and medium loads and lower NOx emissions at higher loads compared to diesel and spark ignition (SI) engines [1-3]. The low reactive fuel (e.g., gasoline) is introduced to fresh air via port fuel injection (PFI) that provides opportunity to form a well-mixed blend of fuel, air and recirculated exhaust gases, if any. The high reactive fuel (e.g., diesel) is early direct injected (DI) inside cylinder during the compression stroke which creates reactivity gradient in the combustion chamber. The controlled reactivity gradient in RCCI engines causes longer combustion duartion and lower pressure rise rates compared to homogeneous charge compression ignition (HCCI) engines [4]. In RCCI engines, ignition initially occurs at small isolated high reactive pockets which continue to grow and merge with other expanding pockets while other ignition pockets emerge [5]. This form of distributed combustion initiation leads to lower gas temperatures compared to CDC which results in a lower heat loss and higher

fuel conversion efficiency. Due to the sensitivity of RCCI reactions to thermal and chemical composition of air fuel mixtures, combustion control of RCCI engines is a major challenge during transient operations. Prior works on RCCI combustion controller design fall into two categories based on the platform for controller implementation and testing. The first category includes RCCI controllers using high fidelity RCCI models to verify controller performance, while the second category included controllers validated on a real RCCI engine.

Among simulation studies, Wu et al. [6] conducted the first RCCI combustion control based on a rule based control design. They studied load transitions on a validated CFD model of an RCCI engine to investigate CA50 trends and developed a control strategy based on adjusting PFI to DI fuel ratio. They used an offline map to design a feedforward steady state controller. Sadabadi et al. [7] developed the first validated physics-based control-oriented model for RCCI combustion. The model in reference [7] could predict start of combustion, burn duration, and CA50 with average tracking errors of 2 CAD. In another simulation based research, Indrajuana et al. [8] formed a function for ignition delay (τ_{id}) , indicated mean effective pressure (IMEP), and premixed ratio (PR) of a validated RCCI engine model that ran with diesel and natural gas fuels. They linearized this function and formed a multiple-input and multiple-output (MIMO) proportional controller to control τ_{id} , IMEP and PR on a multi-zone model. Recently, Indrajuana et al. [9] developed a new controller for switching from conventional dual fuel (CDF) operation to RCCI operation. They used an RCCI engine model and proposed a model-based controller for switching from CDF to RCCI operation.

Second catagory of RCCI combustion controllers design includes studies with RCCI controller implementation on an experimental engine setup. As the first work in this catagory, Arora et al. [10] designed and implemented the first real time transient combustion phasing and load controller for an RCCI engine. They developed two PI controllers to adjust CA50 and IMEP using real time combustion phasing and IMEP calculation from a designed field programmable gate array (FPGA). In another study, Kondipati et al. [11] developed a PI controller for an RCCI engine and used a physics based model to tune the PI controller. Their experimental results proved controller capability to reach desired CA50 in 2-3 engine cycles with an average tracking error of 1 CAD. In another study, Raut et al. [12],[13] designed and implemented the first online MPC on an RCCI engine based on a physics-based control-oriented model. Their controller

[†]Behrouz Khoshbakht Irdmousa, Jeffrey Donald Naber and Mahdi Shahbakhti are with Department of Mechanical Engineering-Engineering Mechanics at Michigan Technological University, {bkhoshi, jnaber, mahdish}@mtu.edu.

^{††}Syed Zeeshan Rizvi is with Corning Incrizvisz@corning.com.

^{†††}Javad Mohammadpour Velni is with School of Electrical & Computer Engineering at the University of Georgia, javadm@uqa.edu.

was designed as a switched MPC controller based on PR values to extend controller range. These works [6–10,12,13] on RCCI combustion control used first principle physical models as the basis to develop control-oriented models. While the physics-based approach is powerful, it requires accurate, control-oriented models which are hard and time consuming to develop. In this situation, data-driven modeling (DDM) approaches can be offered as an alternative. Datadriven approaches do not require thorough knowledge of the underlying physics and can be developed based on available measured data and initial information about involved variables, internal states, and system structure [14]. This paper develops a new DDM for RCCI engine identification and utilizes the data-driven models in an MPC framework [15]. Here, a support vector machine (SVM) based DDM is developed to identify linear parameter-varying (LPV) models for RCCI engine combustion. The LPV framework is selected due to its capability to (i) simplify nonlinear RCCI dynamics into an array of linear models characterized by a scheduling variable, and (ii) guarantee stability of closedloop system for broad range of engine operations. To the best of authors' knowledge, this paper is the first study undertaken to develop a data-driven LPV model to capture RCCI nonlinear dynamics by an easily implementable datadriven LPV model. The new model is used in an MPC framework and verified on a real RCCI engine setup to control CA50 in real time.

This paper is arranged as follows. The engine experimental setup is explained in Section II. Next, the LPV state space model development is discussed in Section III. The MPC controller design and implementation results are presented in Sections IV and V. Finally, conclusions from this study are summarized in Section VI.

II. EXPERIMENTAL SETUP

A GM 2.0L 4-cylinder Ecotec turbocharged Gasoline Direct Injection (GDI) engine was modified to run in RCCI mode. Direct fuel injection pressure is set at 100 bar while port fuel injection runs with 3 bar fuel pressure. Further information on engine specification and setup can be found in reference [12]. During engine modification, low pressure fuel rail and port fuel injectors were added at intake ports to enable RCCI mode operation. *Iso*-octane is injected into intake ports as low reactive fuel and *n*-heptane is injected as high reactive fuel directly into the combustion chamber. Premixed ratio (PR) is used to describe the ratio between low reactive fuel and high reactive fuel. It is defined according to Eq. (1) based on chemical energy from the low reactive fuel divided by the total chemical energy delivered by both fuels.

$$PR = \frac{m_{iso}LHV_{iso}}{m_{iso}LHV_{iso} + m_{nhep}LHV_{nhep}},$$
 (1)

where LHV represents lower heating value of a fuel. A controllable air heater was included at intake air flow path to adjust intake air temperature for RCCI operation. A dSPACE MicroAutoBox (MABX) unit is programmed and used as the

engine control unit (ECU) in addition to dSPACE RapidPro as the power and signal conditioning stage for sensors. Incylinder pressure is measured by PCB piezoelectric pressure transducers. A Spartan-6 field FPGA was programmed in Xilinx to use real time pressure data to compute CA50, and IMEP to provide feedback to the ECU.

Two sets of experiments were conducted in this research. First set of experiments was carried out to obtain training and test data for state space (SS) identification of the RCCI LPV model. In these identification experiments, fuel quantity (FQ) was defined as the scheduling variable since it is the main control variable to adjust engine load (IMEP). Thus, changing FQ leads to changing of the engine load. Measured inputs including PR, FQ, and n-heptane SOI were used along with CA50 as the output to develop a data-driven SS model. The data-driven SS model was then used in conjunction with an MPC controller to form a RCCI combustion controller. The second set of experiments was conducted to evaluate tracking performance of the MPC controller at transient operations. All tests in this research were conducted at 1500 RPM engine speed, without turbocharging and exhaust gas recirculation (EGR) while intake temperature was kept at 333 K $(60^{\circ}C)$.

III. STATE SPACE MODEL IDENTIFICATION

Development of a predictive model to capture RCCI engine combustion is essential for designing RCCI combustion controller for transient operation. It is also important to have a model with low computational demand to be easily implemented on the ECU. DDM approaches can meet these requirements efficiently for less model development costs compared to physics-based approaches. Here, the data-driven SS identification algorithm from reference [16] is adapted for RCCI engine combustion modeling.

Discrete-time LPV models can be described as

$$X_{k+1} = A(p_k)X_k + B(p_k)U_k + K(p_k)E_k,$$

$$Y_k = C(p_k)X_k + E_k,$$
(2)

where X_k , Y_k , and p_k represent the internal states, the outputs, and the time-varying scheduling variable at discrete-time instant k. Additive Gaussian white noise is denoted by E_k . Matrices $A(p_k) \in \mathbb{R}^{n \times n}$, $B(p_k) \in \mathbb{R}^{n \times n_u}$, $K(p_k) \in \mathbb{R}^{n \times n_y}$ and $C(p_k) \in \mathbb{R}^{n_y \times n}$ represent LPV-SS matrices with a functional dependency on the scheduling variable p_k . We can now re-write the LPV-SS model (2) as

$$X_{k+1} = \underbrace{(A(p_k) - K(p_k)C(p_k))}_{\widetilde{A}(p_k)} X_k + B(p_k)U_k + K(p_k)Y_k,$$

$$Y_k = C(p_k)X_k + E_k. \tag{3}$$

The objective here is to identify the functional matrix dependencies $\tilde{A}(p_k)$, $B(p_k)$, $C(p_k)$ based on measured training data $\{X_k, U_k, p_k, Y_k\}_{k=1}^N$ from the plant. A Least-Squares Support Vector Machine (LS-SVM) approach is taken, and

the matrix functions are re-written as

$$X_{k+1} = W_1 \Phi_1(p_k) X_k + W_2 \Phi_2(p_k) U_k + W_3 \Phi_3(p_k) Y_k,$$

$$Y_k = W_4 \Phi_4(p_k) X_k + E_k,$$
(4)

where $W_{1,2,3} \in \mathbb{R}^{n \times n_H}$ and $W_4 \in \mathbb{R}^{n_y \times n_H}$ are unknown weighting matrices, while $\Phi_1(p_k) \in \mathbb{R}^{n_H \times n}$, $\Phi_2(p_k) \in \mathbb{R}^{n_H \times n_u}$, $\Phi_3(p_k) \in \mathbb{R}^{n_H \times n_y}$, and $\Phi_4(p_k) \in \mathbb{R}^{n_H \times n}$ are unknown feature maps with (possibly infinite) dimension n_H . Feature maps can be defined using a kernel function such as polynomial, Gaussian or sigmoid. The following least-squares (LS) objective function is considered:

$$\mathcal{J} = \frac{1}{2} \sum_{i=1}^{4} ||W_i||_{F}^2 + \frac{1}{2} \sum_{k=1}^{N} E_k^{\mathsf{T}} \Gamma E_k, \tag{5}$$

where $||\cdot||_{\mathrm{F}}$ represents Frobenius norm and Γ is the regularization matrix $\mathrm{diag}(\gamma_1,\gamma_2,...,\gamma_{n_y})$ on estimation error E_k . The optimization parameters are the weighting matrices $W_{1,2,3,4}$. Dropping the notation for dependence on p_k for brevity, the problem can be written in the dual form and a Lagrangian function can be written as

$$\mathcal{L}(W_1, W_2, W_3, W_4, \alpha, \beta, E) =$$

$$\mathcal{J} - \sum_{j=1}^{N} \left(\alpha_j^{\top} \{ W_1 \Phi_1 X_j + W_2 \Phi_2 U_j + W_3 \Phi_3 Y_j - X_{j+1} \} \right)$$

$$- \sum_{j=1}^{N} \beta_j^{\top} \{ W_4 \Phi_4 X_j + E_j - Y_{j+1} \}, \tag{6}$$

where $\alpha_j \in \mathbb{R}^n$, $\beta_j \in \mathbb{R}^{n_y}$ are Lagrange multipliers at discrete time j. Lagrangian function has convex form and its global optimum can be found where derivatives are equal to zero.

$$\begin{split} \frac{\partial \mathcal{L}}{\partial \alpha_j} &= 0 \Rightarrow \\ X_{j+1} &= W_1 \Phi_1(p_j) X_j + W_2 \Phi_2(p_j) U_j + W_3 \Phi_3(p_j) Y_j, \end{split} \tag{7a}$$

$$\frac{\partial \mathcal{L}}{\partial W_1} = 0 \Rightarrow W_1 = \sum_{j=1}^{N} \alpha_j X_j^{\top} \Phi_1^{\top}(p_j), \tag{7b}$$

$$\frac{\partial \mathcal{L}}{\partial W_2} = 0 \Rightarrow W_2 = \sum_{j=1}^{N} \alpha_j U_j^{\top} \Phi_2^{\top}(p_j), \tag{7c}$$

$$\frac{\partial \mathcal{L}}{\partial W_3} = 0 \Rightarrow W_3 = \sum_{j=1}^{N} \alpha_j Y_j^{\top} \Phi_3^{\top}(p_j), \tag{7d}$$

$$\frac{\partial \mathcal{L}}{\partial W_4} = 0 \Rightarrow W_4 = \sum_{j=1}^{N} \beta_j X_j^{\top} \Phi_4^{\top}(p_j), \tag{7e}$$

$$\frac{\partial \mathcal{L}}{\partial E_i} = 0 \Rightarrow \beta_j = \Gamma E_j,\tag{7f}$$

$$\frac{\partial \mathcal{L}}{\partial \beta_j} = 0 \Rightarrow Y_j = W_4 \Phi_4(p_j) X_j + E_j. \tag{7g}$$

Substituting (7) into (4), the model can be re-written as

$$\begin{split} X_{k+1} &= \underbrace{\sum_{j=1}^{N} \alpha_j X_j^{\top} \boldsymbol{\Phi}_1^{\top}(p_j)}_{W_1} \boldsymbol{\Phi}_1(p_k) X_k \\ &+ \underbrace{\sum_{j=1}^{N} \alpha_j {U_j}^{\top} \boldsymbol{\Phi}_2^{\top}(p_j)}_{W_2} \boldsymbol{\Phi}_2(p_k) U_k \\ &+ \underbrace{\sum_{j=1}^{N} \alpha_j {Y_j}^{\top} \boldsymbol{\Phi}_3^{\top}(p_j)}_{W_3} \boldsymbol{\Phi}_3(p_k) Y_k, \end{split}$$

$$Y_{k} = \underbrace{\sum_{j=1}^{N} \beta_{j} X_{j}^{\top} \Phi_{4}^{\top}(p_{j})}_{W_{4}} \Phi_{4}(p_{k}) X_{k} + \underbrace{\Gamma^{-1} \beta_{k}}_{E_{k}}.$$
 (8)

Inner product of the feature maps $\Phi_i^{\top}(p_k)\Phi_i(p_j)$ can be expressed by using the so-called kernel trick and defining the following Gramian matrices

$$[\Omega]_{j,k} = \sum_{i=1}^{3} Z_i^{\top}(j)\bar{k}^i(p_j, p_k)Z_i(k),$$
 (9a)

$$[\Xi]_{j,k} = X_j^{\top} \bar{k}^4(p_j, p_k) X_k,$$
 (9b)

where $Z_i(k)$ is X_k, U_k, Y_k for i = 1, 2, 3. In this work, we choose the kernel function $\bar{k}^i(\cdot, \cdot)$ as

$$\bar{k}^{i}(p_{j}, p_{k}) = \exp\left(-\frac{||p_{j} - p_{k}||_{2}^{2}}{2\sigma_{i}^{2}}\right),$$
 (10)

where σ_i is the spread of the Gaussian function and $||\cdot||_2$ denotes \mathcal{L}_2 norm of the vector. We now express (8) in the matrix form as

$$\mathcal{X}_{k+1} = \alpha \Omega,$$

$$\mathcal{Y} = \beta \Xi + \Gamma^{-1} \beta,$$
(11)

where $\Omega \in \mathbb{R}^{N \times N}$ and $\Xi \in \mathbb{R}^{N \times N}$ are kernel matrices defined in (9) and $\alpha = [\alpha_1 \cdots \alpha_N] \in \mathbb{R}^{n \times N}$ and $\beta = [\beta_1 \cdots \beta_N] \in \mathbb{R}^{n_y \times N}$ are Lagrange multipliers. Variables $\mathcal{X}_{k+1} = [X_1 \cdots X_N] \in \mathbb{R}^{n \times N}$ and $\mathcal{Y} = [Y_1 \cdots Y_N] \in \mathbb{R}^{n_y \times N}$ are the states and outputs for the N samples, respectively. Solving (11) for α and β , we obtain

$$\alpha = \mathcal{X}_{k+1} \Omega^{-1},$$

$$\operatorname{vec}(\beta) = \left(I_N \otimes \Gamma^{-1} + \Xi^{\top} \otimes I_{n_y} \right)^{-1} \operatorname{vec}(\mathcal{Y}), \quad (12)$$

where \otimes denotes the Kronecker product and $\operatorname{vec}(\cdot)$ represents the vectorization operator that vertically concatenates columns of a matrix. I_N and I_{n_y} are identity matrices of appropriate dimensions. Using training data $\{X_k, U_k, Y_k\}_{k=1}^N$, $\alpha = [\alpha_1 \cdots \alpha_N]$ and $\beta = [\beta_1 \cdots \beta_N]$ can be computed and

the estimated LPV-SS matrices at Eq. 3 can be written as

$$\tilde{A}_e(\cdot) = W_1 \Phi_1(\cdot) = \sum_{k=1}^N \alpha_k X_k^{\top} \bar{k}^1(p_k, \cdot), \tag{13a}$$

$$B_e(\cdot) = W_2 \Phi_2(\cdot) = \sum_{k=1}^N \alpha_k U_k^{\top} \bar{k}^2(p_k, \cdot),$$
 (13b)

$$K_e(\cdot) = W_3 \Phi_3(\cdot) = \sum_{k=1}^{N} \alpha_k Y_k^{\top} \bar{k}^3(p_k, \cdot),$$
 (13c)

$$C_e(\cdot) = W_4 \Phi_4(\cdot) = \sum_{k=1}^N \beta_k X_k^{\top} \bar{k}^4(p_k, \cdot),$$
 (13d)

where the subscript e denotes estimate. For the case of the RCCI engine, in order to identify the LPV-SS model, we define the states (X), inputs (U), and output (Y) as

$$X = \begin{bmatrix} CA50 & T_{soc} & P_{soc} & IMEP \end{bmatrix}^{\top}, \tag{14a}$$

$$U = \begin{bmatrix} PR & SOI & FQ \end{bmatrix}^{\top}, \tag{14b}$$

$$Y = [CA50]. (14c)$$

As mentioned before, fuel injected per engine cycle, FQ (mg/cycle), is chosen as the scheduling variable. The experimental data are collected and divided into training and test sets. 65% of the data is reserved for training the model and the remaining is used for testing the model. Lagrange multipliers α and β are computed and SS matrices are estimated.

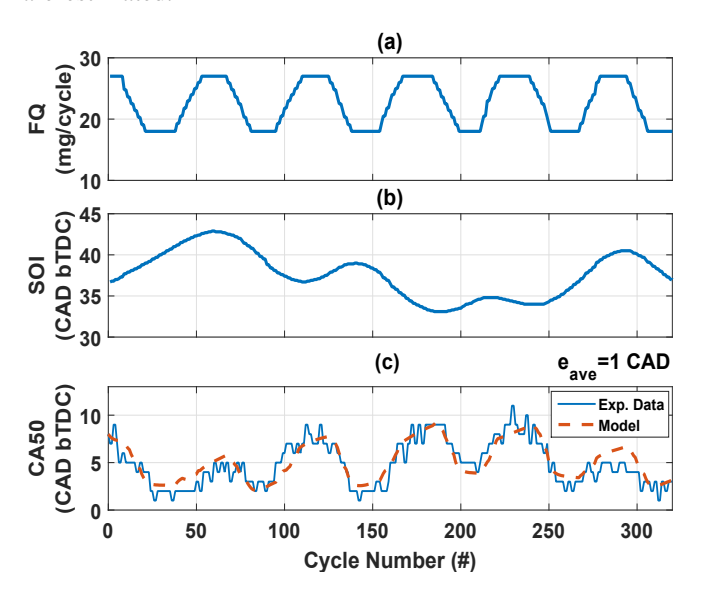


Fig. 1. LPV-SS model validation for $T_{in}=333$ K, N=1500 rpm, $P_{in}=96.5$ kPa, PR=20, 273 kPa $<\!IMEP\!<\!771$ kPa.

Using the computed α and β from (12), the trained model is validated using the test data set. The model is excited using the test inputs and scheduling variable, and CA50 is estimated. These estimated values of CA50 are compared with the measured CA50 for PR=20, as shown in Figure 1. The results show that the developed model can predict CA50 with an average error of 1 CAD. Figure 2 shows

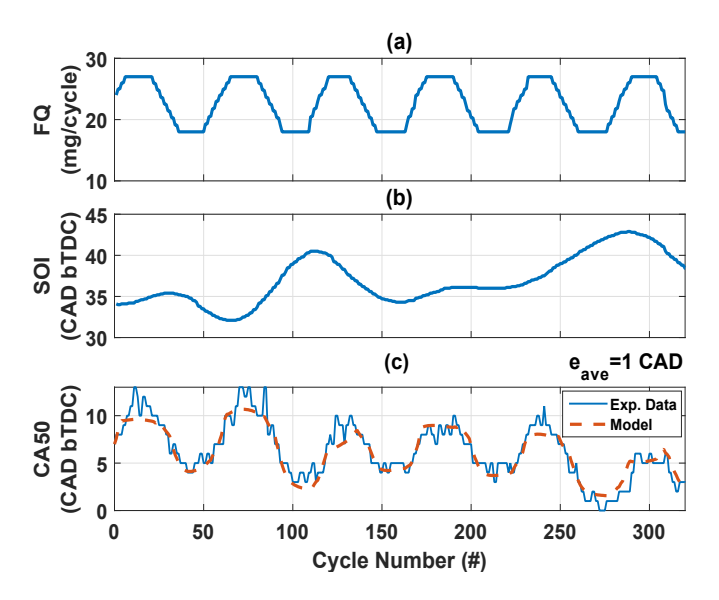


Fig. 2. LPV-SS model validation for $T_{in}=333~{\rm K},~N=1500~{\rm RPM},~P_{in}=96.5~{\rm kPa},~PR=40,~442~{\rm kPa}<IMEP<806~{\rm kPa}.$

similar results for PR=40. These results demonstrate the capability of the identified LPV-SS model to accurately capture the dynamics of the RCCI combustion and the functional dependencies of the model on the FQ. These results show that the model can predict with an acceptable degree of accuracy, the behavior of the RCCI engine, and can thus be used for the synthesis of an LPV MPC control strategy.

IV. MODEL-BASED COMBUSTION CONTROLLER DESIGN

In this work, MPC is chosen as the combustion control strategy due to its capability to consider actuator and state constraints while performing online optimization. Here, an MPC is designed to track desired CA50 by considering 5 engine cycles as prediction horizon to compute optimal *n*-heptane SOI as the control variable. The state space LPV model of the RCCI engine can be represented in discrete time as

$$X_{k+1} = A(FQ)X_k + B(FQ)U_k, \tag{15a}$$

$$Y_{k+1} = C(FQ)X_{k+1} + D(FQ)U_{k+1}, \tag{15b}$$

where states (X), inputs (U), and output (Y) were previously defined by Eq. (14). Based on an iterative calculation, the plant output at prediction horizon can be computed as [17]:

$$\mathbb{Y}_k = FX(k_i) + \Phi \mathbb{U}_k, \tag{16}$$

where

$$Y_k = [Y(k_i + 1|k_i) \ Y(k_i + 2|k_i) \ Y(k_i + 3|k_i) Y(k_i + 4|k_i) \ Y(k_i + 5|k_i)]^\top,$$
(17)

$$\mathbb{U}_{k} = \begin{bmatrix} U(k_{i}) & U(k_{i}+1) & U(k_{i}+3) \\ U(k_{i}+3) & U(k_{i}+4) \end{bmatrix}^{\top},$$
(18)

and $Y(k_i+N|k_i)$ denotes the predicted output at step k_i+N with plant information at step k_i , and $U(k_i+N)$ denotes

control variable at step $k_i + N$. Matrices F and Φ in Eq. (16) are calculated based on A, B, and C matrices from Eq. (15) and are described as

$$F = \begin{bmatrix} CA \\ CA^2 \\ CA^3 \\ CA^4 \\ CA^5 \end{bmatrix}; \Phi = \begin{bmatrix} CB & 0 & 0 & 0 & 0 \\ CAB & CB & 0 & 0 & 0 \\ CA^2B & CAB & CB & 0 & 0 \\ CA^3B & CA^2B & CAB & CB & 0 \\ CA^4B & CA^3B & CA^2B & CAB & CB \end{bmatrix}$$
(19)

where notation for dependence of matrices on FQ was dropped for brevity. An MPC cost function is defined to minimize prediction tracking error and control action magnitude as

$$J = \sum_{i=1}^{N} [(\Psi_i - Y_i)^{\top} Q(\Psi_i - Y_i) + U_i^{\top} R U_i],$$
 (20)

where the Ψ is defined as the reference outputs over the prediction horizon, Q is the weighting matrix on tracking errors and R is the weighting matrix on the magnitude of control variables through the prediction horizon. The optimal solution to control variable matrix $\mathbb U$ to minimize cost function (20) can be derived as

$$\mathbb{U} = (\Phi^T Q \Phi + R)^{-1} \Phi^\top Q (\Psi - F X_k). \tag{21}$$

The MPC cost function for constrained conditions can be expressed by

$$J = \frac{1}{2} \mathbb{U}^{\top} E \mathbb{U} + \mathbb{U}^{\top} H, \tag{22}$$

where matrices E and H are determined by

$$E = (\Phi^{\top} Q \Phi + R), \tag{23}$$

$$H = \Phi^{\top} Q(\Psi - FX_k). \tag{24}$$

Constraints are defined by Eq. (25) for control commands to actuators and magnitude of output states to protect RCCI engine from receiving excessive control commands.

$$A_{cons}U \leqslant B_{cons},$$
 (25)

where

$$A_{cons} = \begin{bmatrix} I_{10 \times 10} \\ -I_{10 \times 10} \end{bmatrix}; B_{cons} = \begin{bmatrix} U_{max} - u(k_i - 1) \\ U_{min} + u(k_i - 1) \end{bmatrix}. (26)$$

Figure 3 shows the LPV MPC controller schematic and its connections with the RCCI engine and the FPGA. The ECU is loaded with the LPV plant model, a Kalman filter, and the MPC controller. The MPC controller receives identified SS plant matrices as well as states and input values to compute optimal n-heptane SOI values based on Eq. (21) as the optimal MPC solution. SS matrices are provided to the MPC controller from the trained LPV model. SS models are dependent on FQ as the scheduling variable which is assigned based on the engine load. The Kalman filter is utilized to estimate T_{soc} and P_{soc} states which are difficult to measure. Only the first step value for calculated optimal n-heptane SOI is implemented and the rest of calculated SOIs are updated in the next time steps.

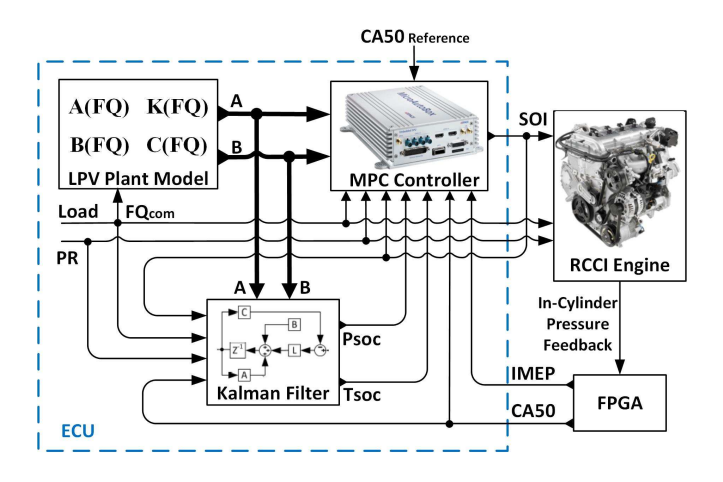


Fig. 3. Schematic of the designed LPV MPC controller.

V. EXPERIMENTAL RESULTS

In this section, the combustion controller performance is evaluated under transient conditions. Figure 4 presents CA50 tracking results for controller performance at a constant fuel quantity condition. It demonstrates the controller's capability to track desired CA50 with 0.7 CAD average error by adjusting SOI as the control variable. By comparing data-

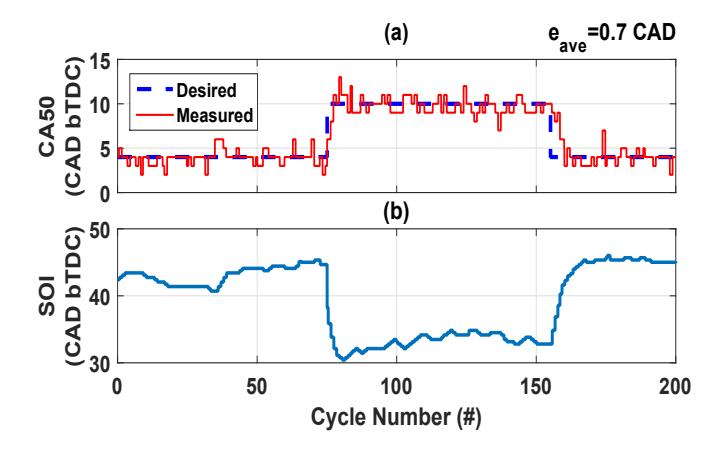


Fig. 4. Controller performance in tracking desired combustion phasing with $T_{in}=333\,$ K, $N=1500\,$ RPM, $P_{in}=96.5\,$ kPa, $FQ=25\,$ mg/cycle.

driven combustion control results with the physics-based combustion control results for the same engine which were presented by Raut et al. [12], it can be observed that data-driven combustion phasing controller in this paper has similar average tracking error compared to the physics-based method in [12]. Considering the efforts required for developing physics-based control-oriented models, these results demonstrate the advantage of data-driven methods over physics-based controller designs due to their shorter development time and similar tracking performance.

Figure 5 presents controller tracking performance for varying FQ quantities. FQ is increased step-wise from 20 to 28 mg/cycle. The engine model is defined for combustion controller by the data-driven model at each step. Desired

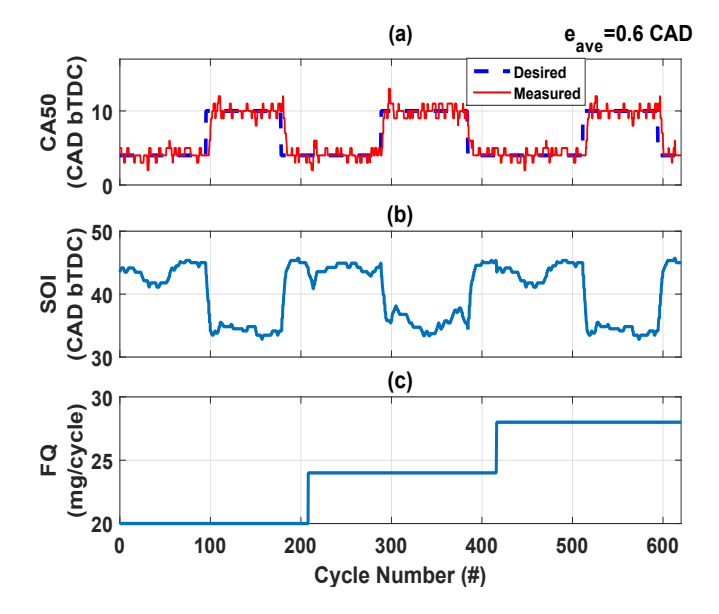


Fig. 5. Combustion control performance with variable FQ, constant $PR=20,\,T_{in}=333\,$ K, $N=1500\,$ RPM, and $P_{in}=96.5\,$ kPa.

CA50 is also changed at each step and controller adjusts *n*-heptane SOI to track the desired CA50. Closed loop response results show that desired CA50 is tracked with an average error of 0.6 CAD. Combustion controller results in Figure 5 demonstrate that the learned LPV model can switch between SS models correctly based on scheduling variable and the MPC controller is capable of reaching the desired CA50 with small tracking error within 3 engine cycles.

VI. SUMMARY AND CONCLUSION

This paper introduced the first data-driven LPV model for an RCCI engine using the method of least-squares support vector machines. Experimental measurements of the RCCI engine inputs (i.e., SOI, PR, FQ) and the desired output (i.e., CA50) were used to develop the LPV model. This model used FO (related to engine load) as the scheduling variable and determined CA50 as a function of three control inputs. The data-driven model was employed to estimate CA50 by using measured engine inputs from another experimental data set and was validated based on comparing estimated CA50 results with measured CA50 values. Validation results showed that the estimated state space LPV model could predict combustion phasing (CA50) with an average error less than 1 CAD. The LPV model was then incorporated into an MPC framework to control CA50 by modifying start of injection (SOI) of n-heptane as the DI fuel. Experimental results for the controller demonstrated that the LPV based MPC controller was able to track desired CA50 with a maximum of 0.7 CAD average error for varying engine conditions. These experimental results demonstrated that data-driven MPC combustion controller can provide similar results compared to physics-based MPC combustion controller while requiring less development time.

ACKNOWLEDGMENT

This research is partially supported by the United States National Science Foundation (Grant # 1762520). The authors acknowledge Karan Dhankani, Akshat Raut, and Paul Dice from Michigan Tech. University for their help in RCCI LPV modeling, MPC design, and engine setup preparation, respectively.

REFERENCES

- E. Ansari, K. Poorghasemi, B. Khoshbakht Irdmousa, M. Shahbakhti, and J. Naber, "Efficiency and emissions mapping of a light duty dieselnatural gas engine operating in conventional diesel and RCCI modes," SAE International, 2016, Paper No. 2016-01-2309.
- [2] E. Ansari, M. Shahbakhti, and J. Naber, "Optimization of performance and operational cost for a dual mode diesel-natural gas RCCI and diesel combustion engine," *Applied Energy*, vol. 231, pp. 549–561, 2018.
- [3] K. Poorghasemi, R. K. Saray, E. Ansari, B. K. Irdmousa, M. Shah-bakhti, and J. D. Naber, "Effect of diesel injection strategies on natural gas/diesel RCCI combustion characteristics in a light duty diesel engine," *Applied Energy*, vol. 199, pp. 430–446, 2017.
- [4] A. B. Dempsey, N. R. Walker, and R. Reitz, "Effect of piston bowl geometry on dual fuel reactivity controlled compression ignition (RCCI) in a light-duty engine operated with gasoline/diesel and methanol/diesel," SAE International Journal of Engines, vol. 6, no. 1, pp. 78–100, 2013.
- [5] S. L. Kokjohn, M. P. Musculus, and R. D. Reitz, "Evaluating temperature and fuel stratification for heat-release rate control in a reactivitycontrolled compression-ignition engine using optical diagnostics and chemical kinetics modeling," *Combustion and Flame*, vol. 162, no. 6, pp. 2729–2742, 2015.
- [6] Y. Wu, R. Hanson, and R. D. Reitz, "Investigation of combustion phasing control strategy during reactivity controlled compression ignition (RCCI) multi-cylinder engine load transitions," *Journal of Engineering for Gas Turbines and Power*, vol. 136, no. 9, p. 091511, 2014.
- [7] K. Khodadadi Sadabadi, M. Shahbakhti, A. N. Bharath, and R. D. Reitz, "Modeling of combustion phasing of a reactivity-controlled compression ignition engine for control applications," *International Journal of Engine Research*, vol. 17, no. 4, pp. 421–435, 2016.
- [8] A. Indrajuana, C. Bekdemir, X. Luo, and F. Willems, "Robust multivariable feedback control of natural gas-diesel RCCI combustion," IFAC-PapersOnLine, vol. 49, no. 11, pp. 217–222, 2016.
- [9] A. Indrajuana, C. Bekdemir, E. Feru, and F. Willems, "Towards model-based control of RCCI-CDF mode-switching in dual fuel engines," SAE International, 2018, Paper no. 2018-01-0263.
- [10] J. K. Arora and M. Shahbakhti, "Real-time closed-loop control of a light-duty RCCI engine during transient operations," SAE International, 2017, Paper No. 2017-01-0767.
- [11] N. N. T. Kondipati, J. K. Arora, M. Bidarvatan, and M. Shahbakhti, "Modeling, design and implementation of a closed-loop combustion controller for an RCCI engine," in *American Control Conference*, 2017, pp. 4747–4752.
- [12] A. Raut, B. Khoshbakht Irdmousa, and M. Shahbakhti, "Dynamic modeling and model predictive control of an RCCI engine," *Control Engineering Practice*, vol. 81, pp. 129–144, 2018.
- [13] A. Raut, M. Bidarvatan, H. Borhan, and M. Shahbakhti, "Model predictive control of an RCCI engine," in 2018 Annual American Control Conference (ACC), 2018, pp. 1604–1609.
- [14] M. Tanaskovic, L. Fagiano, C. Novara, and M. Morari, "Data-driven control of nonlinear systems: An on-line direct approach," *Automatica*, vol. 75, pp. 1–10, 2017.
- [15] D. Solomatine, L. M. See, and R. Abrahart, "Data-driven modelling: concepts, approaches and experiences," in *Practical Hydroinformatics*. Springer, 2009, pp. 17–30.
- [16] S. Z. Rizvi, J. Mohammadpour, R. Tóth, and N. Meskin, "A kernel-based approach to MIMO LPV state-space identification and application to a nonlinear process system," *IFAC-PapersOnLine*, vol. 48, no. 26, pp. 85–90, 2015.
- [17] L. Wang, Model Predictive Control System Design and Implementation using MATLAB®. Springer Science & Business Media, 2009, Chapter 1.